Continuum model of mode-III crack propagation with surface friction

Hiizu Nakanishi
Department of Physics, Faculty of Science and Technology, Keio University, Yokohama 223, Japan
(Received 15 December 1993)

A two-dimensional model of mode-III crack propagation with a velocity strengthening surface friction is investigated theoretically. Using the Wiener-Hopf technique developed by Langer and Nakanishi [Phys. Rev. E **48**, 439 (1993)] with the condition that the stress should not diverge at the crack tip, we determine the crack propagation speed for given external load. It is shown that the maximum crack speed is slower than the sound speed contrary to the case studied by Langer and Nakanishi. Is is also demonstrated that the crack speed does not grow quickly as the externally applied stress is increased beyond a threshold stress if the friction stress is comparable with the distortion stress. In the case of no cohesive stress, a divergence around the crack tip exists, but the velocity strengthening friction makes it weaker than the ordinary inverse square root divergence.

PACS number(s): 62.20.Mk, 46.30.Nz, 81.40.Np, 91.30.Bi

I. INTRODUCTION

Propagation of a single straight crack is the simplest problem of fracture dynamics. A difficulty of fracture dynamics is that even such an "elementary" process involves a variety of processes and has not been fully understood yet.

In conventional theory based on elastodynamics [1], crack tip motion is analyzed using the energy balance condition that the energy flow into the crack tip should be equal to the energy required to open a new surface. Such a theory gives the Rayleigh surface wave speed as the maximum crack speed. On the other hand, the experimentally observed maximum crack speed is often far below the Rayleigh speed [2], and it has also been reported that steady crack propagation could be dynamically unstable [3]. Such an instability is difficult to understand within the conventional framework of elastodynamics. There are also numerical simulations that show crack propagation much slower than the sound speed [4].

Recently several theoretical analyses [5–11] have been done from a more "microscopic" point of view and it has been pointed out that dissipation could have an important effect on crack propagation [7–9,11].

In this paper, we study the effects of surface friction on crack propagation theoretically. We consider the simplest case, namely, steady propagation of a single straight mode-III crack in a two-dimensional elastic material with cohesive stress and surface dissipation. This type of model has been studied recently by Langer and Nakanishi (LN) [9] and they have developed a Wiener-Hopf technique to obtain steady solutions, a technique which will be used for the present model.

The difference between the present model and that of LN is that they considered the surface dissipation caused by a viscosity term while we consider surface friction. LN pointed out that viscous dissipation acts as a singular perturbation in the model and could bring about an effective threshold for an external load to induce crack propagation. This effective threshold can be much larger than the Griffith threshold determined by energy balance. They also found that supersonic crack propagation accompanied by shock wave radiation is possible for the model. In the present model, on the other hand, dissipation comes from the surface friction that is proportional to the slipping velocity. This term is not a singular perturbation but we will show that it has some remarkable effects on crack propagation.

The main results for the present model are the following. Without cohesive stress, the divergence of the stress at the crack tip cannot be removed, but the friction stress makes this divergence weaker than the ordinary $1/\sqrt{x}$ divergence. With cohesive stress, the divergence can be eliminated by choosing a proper crack speed for a given external load. By using the condition that the divergence should not appear, the crack speed is determined as a function of external load and it is shown that the maximum crack speed is smaller than the sound speed; supersonic crack propagation is not possible. When the friction is weak, the maximum crack speed is close to the sound speed and the crack speed reaches the maximum speed as soon as the external load exceeds the Griffith threshold, but for stronger friction the maximum speed could be substantially smaller than the sound speed, and the crack speed remains small until the externally applied stress is increased close to the yield stress.

The paper is organized as follows. The model is introduced in Sec. II and the equations to be solved by the Wiener-Hopf method are derived in Sec. III. In Sec. IV, the Wiener-Hopf solutions without and with cohesive stress are obtained, using the formulation developed by LN. Asymptotic forms and numerical estimates of the solutions are given in Sec. V and the last section comprises a short discussion.

II. MODEL

The system we study is a single straight mode-III crack in a two-dimensional elastic material (Fig. 1). We only consider an antiplane displacement $u(x,y,t)$ to simplify

TABLE I. The correspondence between the variables in the original unit system and those in the dimensionless unit system. W is a length scale defined by $W \equiv c_0/\omega_0$. Expressions in the original unit can be obtained from dimensionless expressions by replacing the lower variables with the upper ones.

Original unit	x/W, y/W	$\omega_0 t$	$(\mu/W)u$, $(\mu/W)\Delta$, $(\mu/W)\delta$	v/c_0	$(W\omega_0/\mu)\alpha$	σ
Dimensionless unit	x, y	t	u, Δ, δ	v	α	σ

the analysis, and the displacement is assumed to follow the equation of motion

$$\ddot{u}(x,y,t) = c_0^2\nabla^2 u(x,y,t) - \omega_0^2(u(x,y,t) \mp \Delta) \qquad (y \gtrless 0)\ , \quad (1)$$

where the dots denote the time derivative and c_0 stands for the sound speed. The last term in the right hand side represents the external load to drive a crack running along the x axis; $\pm\Delta$ is the displacement imposed on the system at $y \gtrless 0$, and ω_0 is the angular velocity of the uniform oscillation around $u = \pm\Delta$. This type of loading may not be possible for most experimental configurations, but for large values of $W \equiv c_0/\omega_0$ the distortion along the x axis is similar to that of ordinary loading, namely, similar to the situation where a strip of elastic sheet with width W is being displaced at the edges by Δ.

The crack is assumed to run along the x axis in the $-x$ direction with the crack tip position $(x_{\rm tip}(t), 0)$. Thus the displacement along the x axis is expressed as

$$u(x, y = +0, t) = \begin{cases} 0 & [x \le x_{\rm tip}(t)] \\ U(x,t) & [x > x_{\rm tip}(t)] \end{cases}, \quad (2)$$

where $U(x,t)$ is half of a crack opening. We only need to consider the upper half plane ($y \ge 0$) due to the symmetry.

The stress along the x axis is also needed to solve the problem, and is given by

$$\mu \left.\frac{\partial u}{\partial y}\right|_{y=+0} = \begin{cases} \sigma(x,t) & [x \le x_{\rm tip}(t)] \\ \sigma_c(U(x,t)) + \alpha\dot{U}(x,t) & [x > x_{\rm tip}(t)] \end{cases}, \quad (3)$$

where μ is the elastic modulus, $\sigma(x,t)$ is the stress ahead of the crack tip, and $\sigma_c(U)$ is the cohesive stress that depends upon the displacement $U(x,t)$. The term $\alpha\dot{U}(x,t)$ with the positive constant $\alpha > 0$ represents velocity strengthening friction stress acting on the crack surface, the effect of which on the crack propagation is the subject of the present work.

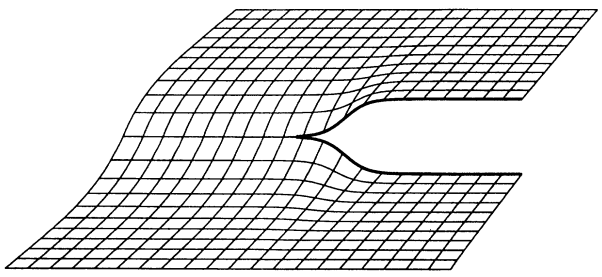

FIG. 1. Mode-III crack propagation in a two-dimensional elastic sheet.

We have formulated our problem to solve Eq. (1) with the boundary conditions (2) and (3). What is peculiar to the present type of problem is that the functions $U(x,t)$ and $\sigma(x,t)$ in the boundary conditions are unknown and should be determined by solving the problem. The Wiener-Hopf method can be used for this type of boundary condition problem and the technique has been developed by LN to obtain a steady solution.

To simplify notation, we will employ the unit system where $c_0 = \omega_0 = \mu = 1$ except for the last section. The expressions in the original unit system can be recovered from the dimensionless expressions by using the correspondence in Table I.

III. STEADY SOLUTION OF PROPAGATING CRACK

We look for the steady solution which represents the propagating crack in the $-x$ direction at constant speed v, namely, the solution depends on x and t only in the form of $x + vt$. Thus, in the coordinate system moving with the crack at the origin, Eqs. (1), (2), and (3) become

$$\left(\beta^2\frac{\partial^2}{\partial x^2} + \frac{\partial^2}{\partial y^2}\right)u(x,y) - [u(x,y) - \Delta] = 0 \quad (y > 0)\ , \quad (4)$$

$$u(x, y = +0) = \begin{cases} 0 & (x \le 0) \\ U(x) & (x > 0) \end{cases}, \quad (5)$$

$$\left.\frac{\partial u}{\partial y}\right|_{y=+0} = \begin{cases} \sigma(x) & (x \le 0) \\ \sigma_c(U(x)) + \alpha v U'(x) & (x > 0) \end{cases}, \quad (6)$$

where

$$\beta \equiv \sqrt{1 - v^2}, \quad (7)$$

and the prime denotes the x derivative. We have assumed that v is smaller than the sound speed, or smaller than 1 in the units used here. We will see that the maximum possible crack speed is smaller than the sound speed.

By introducing a new variable

$$\xi \equiv x/\beta, \quad (8)$$

Eqs. (4) and (6) are expressed as

$$\left(\frac{\partial^2}{\partial\xi^2}+\frac{\partial^2}{\partial y^2}\right)u(\xi,y)-[u(\xi,y)-\Delta]=0 \qquad (y>0), \tag{9}$$

$$\left.\frac{\partial u}{\partial y}\right|_{y=+0}=\begin{cases}\sigma(\xi) & (\xi\le 0)\\ \sigma_c(U(\xi))+\tilde{\alpha}U'(\xi) & (\xi>0)\end{cases}, \tag{10}$$

where

$$\tilde{\alpha}\equiv\alpha v/\beta. \tag{11}$$

From these equations, it becomes obvious that α and v dependence comes into the problem only in the form of $\tilde{\alpha}$ defined by Eq. (11).

The formal solution of Eq. (9) with the boundary condition (5) is written as

$$u(\xi,y)=\Delta(1-e^{-y})+\int\frac{dk}{2\pi}\hat{U}^{(+)}(k)e^{-\hat{K}(k)y+ik\xi} \tag{12}$$

with

$$\hat{K}(k)\equiv\sqrt{1+k^2}; \qquad \mathrm{Re}\hat{K}(k)\ge 0\ , \tag{13}$$

where $\hat{U}^{(+)}(k)$ is the Fourier transform of $U(\xi)$. The superscript $(+)$ denotes that $U(\xi)$ is nonzero only for $\xi>0$; consequently, $\hat{U}^{(+)}(k)$ is regular in the lower half of the complex k plane. The superscript $(-)$ will be used for the opposite.

Then the boundary condition (10) is translated as

$$-\hat{Q}(k)\hat{U}^{(+)}(k)-\frac{i\Delta}{k-i\epsilon}-\hat{\sigma}_c^{(+)}(k)=\hat{\sigma}^{(-)}(k)-\frac{i\Delta}{k+i\epsilon}\ , \tag{14}$$

$$\hat{Q}(k)\equiv\hat{K}(k)+\tilde{\alpha}ik, \tag{15}$$

where ϵ is a positive infinitesimal and $\hat{\sigma}^{(-)}(k)$ is the Fourier transform of $\sigma(\xi)$. $\hat{\sigma}_c^{(+)}(k)$ is defined by

$$\hat{\sigma}_c^{(+)}(k)\equiv\int_0^\infty d\xi e^{-ik\xi}\sigma_c(U(\xi)). \tag{16}$$

IV. WIENER-HOPF SOLUTIONS

From Eq. (14) we should determine both $\hat{U}^{(+)}(k)$ and $\hat{\sigma}^{(-)}(k)$. This can be done using the Wiener-Hopf method [12] following the procedure developed by LN [9].

The essential part of the problem is how to factorize $\hat{Q}(k)$ into two functions: the one, $\hat{Q}^{(+)}(k)$, regular in the lower half plane and the other, $\hat{Q}^{(-)}(k)$, regular in the upper half plane. In the Appendix it is shown that $\hat{Q}(k)$ can be factorized as

$$\hat{Q}(k)\equiv\hat{Q}^{(+)}(k)\hat{Q}^{(-)}(k)\,, \tag{17}$$

$$\hat{Q}^{(+)}(k)\equiv\frac{k_0-k}{k_0}\exp[\hat{\Phi}^{(+)}(k)]\,, \tag{18}$$

$$\hat{Q}^{(-)}(k)\equiv\exp[\hat{\Phi}^{(-)}(k)]\,, \tag{19}$$

$$\hat{\Phi}^{(\pm)}(k)\equiv\mp\int_1^\infty\frac{dp}{\pi}\left(\frac{1}{p}-\frac{1}{p\pm ik}\right)\theta(p),$$
$$\theta(p)\equiv\tan^{-1}\left(\frac{\sqrt{p^2-1}}{\tilde{\alpha}p}\right), \tag{20}$$

where k_0 is a solution of $\hat{Q}(k)=0$ and is given by

$$k_0=i\Big/\sqrt{1+\tilde{\alpha}^2}\equiv ip_0\,.$$

Note that $\hat{Q}^{(\pm)}(k)$ are normalized as

$$\hat{Q}^{(+)}(0)=\hat{Q}^{(-)}(0)=1.$$

For the large $|k|$ limit, their asymptotic behaviors can be shown to be

$$\hat{Q}^{(+)}(k)\sim k^{1-\chi}, \qquad \hat{Q}^{(-)}(k)\sim k^{\chi}, \tag{21}$$

where

$$\chi\equiv\frac{1}{2}-\frac{1}{\pi}\tan^{-1}\tilde{\alpha}\,. \tag{22}$$

In the following, we will employ the formulation developed by LN.

A. $\sigma_c=0$ case

First, in order to see some effects of the friction, we discuss the case without cohesive stress, namely, $\sigma_c=0$, in which case the solutions are denoted by U_0 and σ_0. The Wiener-Hopf decomposition gives

$$\hat{U}_0^{(+)}(k)=\frac{-1}{\hat{Q}^{(+)}(k)}\left(\frac{i\Delta}{k-i\epsilon}+\hat{M}(k)\right), \tag{23}$$

$$\hat{\sigma}_0^{(-)}(k)=\frac{i\Delta}{k+i\epsilon}-\hat{Q}^{(-)}(k)\times\left[\frac{i\Delta}{k}\left(\frac{1}{\hat{Q}^{(-)}(k)}-1\right)-\hat{M}(k)\right], \tag{24}$$

where $\hat{M}(k)$ is an entire function to be determined through physical considerations. If we require that $U_0(\xi)\to 0$ as $\xi\to+0$, we obtain

$$\hat{M}(k)\equiv 0.$$

If we define

$$S(\xi)\equiv\int\frac{dk}{2\pi}\frac{e^{ik\xi}}{\hat{Q}^{(+)}(k)}\,, \tag{25}$$

then $U_0(\xi)$ is expressed as

$$U_0'(\xi)=\Delta S(\xi). \tag{26}$$

The asymptotic behaviors around the crack tip are obtained from Eq. (21) as

$$U_0(x) \sim x^{1-\chi}, \qquad \sigma_0(x) \sim |x|^{-\chi}, \tag{27}$$

where we have used Eq. (8). They should be compared with the ordinary behavior without the friction term,

$$U_{00}(x) \sim \sqrt{x}, \qquad \sigma_{00}(x) \sim 1/\sqrt{|x|}. \tag{28}$$

Since $0 < \chi < 1/2$ from Eq. (22), the velocity strengthening surface friction makes the crack tip singularity weaker than the ordinary one that is described by a stress intensity factor. Numerical estimates of $\sigma_0(x)$ and $U_0(x)$ are shown in Fig. 2 for $\alpha = 1$ and v =0.1, 0.5, and 0.9 on a logarithmic scale.

B. $\sigma_c \neq 0$ case

In the presence of the σ_c term, this divergence can be eliminated by chosing an appropriate crack speed v as we will see. The Wiener-Hopf decomposition of Eq. (14) gives

$$\hat{U}^{(+)}(k) = \frac{-1}{\hat{Q}^{(+)}(k)}\left[\frac{i\Delta}{k-i\epsilon} + \hat{\Lambda}^{(+)}(k)\right], \tag{29}$$

$$\hat{\sigma}^{(-)}(k) = \frac{i\Delta}{k+i\epsilon} - \hat{Q}^{(-)}(k) \times \left[\frac{i\Delta}{k}\left(\frac{1}{\hat{Q}^{(-)}(k)} - 1\right) + \hat{\Lambda}^{(-)}(k)\right], \tag{30}$$

where

$$\hat{\Lambda}^{(\pm)}(k) \equiv \mp \int_{C^{(\pm)}} \frac{dz}{2\pi i} \frac{1}{z-k} \frac{\hat{\sigma}_c^{(+)}(z)}{\hat{Q}^{(-)}(z)}, \tag{31}$$

and $C^{(+)}$ ($C^{(-)}$) is an integral path that runs infinitesimally above (below) the real axis (Fig. 3). In deriving Eqs. (29) and (30), we have set the undetermined entire function $\hat{M}(k) = 0$, using the same argument as that in the $\sigma_c = 0$ case.

In the presence of the cohesive force, we can impose the condition that the stress ahead of the crack tip $\sigma(\xi)$ should not diverge as $\xi \to -0$. In Fourier space, this condition is translated as

$$\hat{\sigma}^{(-)}(k) \lesssim O\left(\frac{1}{k}\right) \qquad (|k| \to \infty), \tag{32}$$

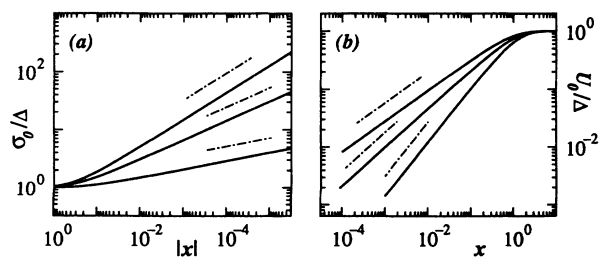

FIG. 2. The log-log plot of stress $\sigma(x)$ (a) and crack opening $U_0(x)$ and (b) in the case of no cohesive stress for $\alpha = 1$ and v =0.1, 0.5, and 0.9 from top to bottom. The dotted-dashed lines represent the slopes $-\chi$ (a) and $1-\chi$ (b) for each parameter.

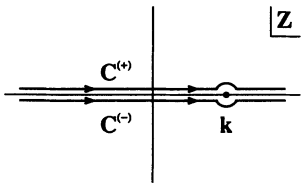

FIG. 3. The integral paths $C^{(\pm)}$ in the complex z plane.

and the expansion of $\hat{\Lambda}^{(-)}(k)$ in powers of $1/k$ gives us

$$\Delta = \int_0^\infty d\xi \sigma_c(U(\xi)) T(\xi), \tag{33}$$

where

$$T(\xi) \equiv \int \frac{dk}{2\pi} \frac{e^{-ik\xi}}{\hat{Q}^{(-)}(k)}. \tag{34}$$

With this relation (33), $\hat{U}^{(+)}(k)$ of Eq. (29) can be transformed into real space as

$$U'(\xi) = -\int_0^\xi d\xi' S(\xi - \xi') \times \int_{\xi'}^\infty d\xi'' T(\xi'' - \xi') \frac{d}{d\xi''} \sigma_c(U(\xi'')) . \tag{35}$$

Equations (33) and (35) are coupled through $U(\xi)$, and the crack speed v comes into the equations through $\tilde{\alpha}$ and ξ; thus v can be determined from Eqs. (33) and (35) as a function of the external load Δ for a given set of material parameters, namely, α and the parameters that characterize $\sigma_c(U)$.

V. NUMERICAL ANALYSIS FOR A SIMPLE COHESIVE STRESS

It is possible to estimate Eqs. (33) and (35) in the case of the simple cohesive stress given by

$$\sigma_c(U) = \begin{cases} \sigma_y & (0 \le U \le \delta) \\ 0 & (U > \delta), \end{cases} \tag{36}$$

where σ_y is a yield stress and δ is the region of the cohesive stress (Fig. 4). Note that the energy needed to open

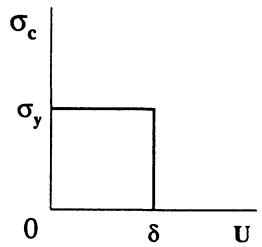

FIG. 4. The cohesive stress σ_y as a function of the displacement U.

the crack is twice $\delta\sigma_y$ per unit length for this cohesive stress.

Then the condition (33) becomes

$$\frac{\Delta}{\sigma_y} = \int_0^{\xi_\ell} d\xi T(\xi), \tag{37}$$

where

$$\xi_\ell \equiv \ell/\sqrt{1-v^2} \tag{38}$$

and ℓ is the length of the cohesive region. This length of the cohesive region should be determined by

$$U(\xi_\ell) = \delta,$$

which turns out to be

$$\frac{\delta}{\sigma_y} = \int_0^{\xi_\ell} d\xi T(\xi) \int_0^{\xi} d\xi' S(\xi') \tag{39}$$

from Eqs. (35) and (36).

For given material parameters σ_y, δ, and α, the crack speed v and the cohesive region length ℓ can be determined as functions of the external load Δ from Eqs. (37) and (39).

(1) Griffith threshold. In the $v \to 0$ limit, the functions $S(\xi)$ and $T(\xi)$ become

$$S(\xi) = T(\xi) = e^{-\xi}\Big/\sqrt{\pi\xi} \quad (v=0)\ ; \tag{40}$$

thus, from Eqs. (37) and (39) we obtain the Griffith condition $\Delta = \Delta_G$ with

$$\tfrac{1}{2}\Delta_G^2 = \delta\sigma_y, \tag{41}$$

namely, the crack starts moving when the crack opening energy balances with the elastic energy stored in the material. We call the threshold Δ_G the Griffith threshold.

(2) Maximum crack speed. The largest possible external load is σ_y, beyond which the material breaks everywhere and a propagating crack is not possible. At $\Delta = \sigma_y$, $\xi_\ell \to \infty$ because of Eq. (37) and the integral

$$\int_0^{\infty} d\xi T(\xi) = \frac{1}{\hat{Q}^{(-)}(0)} = 1. \tag{42}$$

Thus, in this limit, Eq. (39) becomes

$$\frac{\delta}{\sigma_y} = \int_0^{\infty} d\xi T(\xi) \int_0^{\xi} d\xi' S(\xi') = \frac{1}{2}\left[1 - \frac{\tilde{\alpha}_{\max}}{\sqrt{\tilde{\alpha}_{\max}^2+1}}\right]. \tag{43}$$

For a given value of δ/σ_y, we can obtain from Eq. (43) the maximum value of $\tilde{\alpha}$, or $\tilde{\alpha}_{\max}$, from which the maximum crack speed $v_{\max}$ is calculated for given α. Note that δ/σ_y cannot be larger than 1/2 in the present model.

In Fig. 5, $v_{\max}$ is shown as a function of α for δ/σ_y=0.01 (a), 0.001 (b), and 0.0001 (c). The maximum crack speed $v_{\max}$ goes to the sound speed in the $\delta/\sigma_y \to 0$ limit, but it can be substantially smaller than the sound speed for large α and relatively large δ/σ_y.

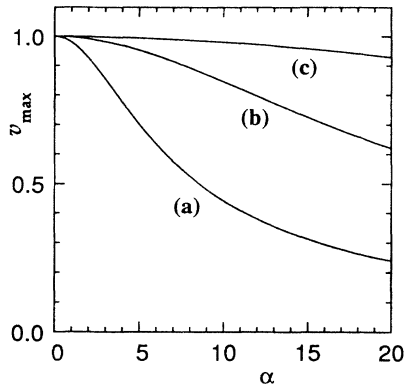

FIG. 5. The maximum crack speed $v_{\max}$ vs α for δ/σ_c =0.01 (a), 0.001 (b), and 0.0001 (c).

(3) Asymptotic expressions. When δ/σ_y is small, then $\xi \ll 1$ and the asymptotic expressions for Eqs. (37) and (39) can be obtained as

$$\frac{\Delta}{\Delta_G} = \frac{\Gamma(1-\chi)}{\sqrt{2\pi\chi}\sqrt{1+\tilde{\alpha}^2}} \exp\left(-\chi + \frac{1}{2\sqrt{1+\tilde{\alpha}^2}}\right) \times \left[(1-\chi)\pi\sin(\pi\chi)\left(1+\tilde{\alpha}^2\right)^{3/2}\right]^{\chi} \left(\frac{\delta}{\sigma_y}\right)^{\chi-1/2}, \tag{44}$$

$$\ell = \beta(1-\chi)\pi\sin(\pi\chi)\left(1+\tilde{\alpha}^2\right)^{3/2}\left(\frac{\delta}{\sigma_y}\right), \tag{45}$$

where $\Gamma(x)$ is the gamma function. These expressions are valid for

$$\frac{\alpha v}{\sqrt{1-v^2}}\left(\frac{\delta}{\sigma_y}\right) \ll 1. \tag{46}$$

(4) Crack speed. The numerically estimated crack speed v is plotted against Δ/Δ_G on a semilogarithmic scale for δ/σ_y=0.001 and α = 0.1 (a), 1 (b), 3 (c), and 10 (d) in Fig. 6 with the asymptotic expression (44).

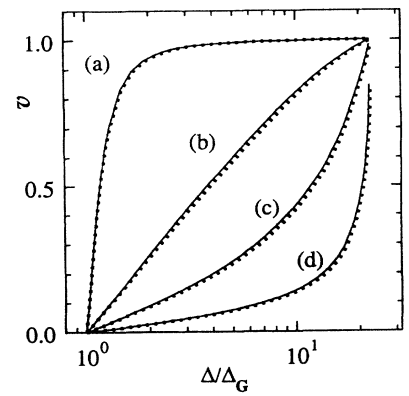

FIG. 6. The crack speed v vs the external load Δ/Δ_G on semilog scale for δ/σ_c = 0.001 and α =0.1 (a), 1 (b), 3 (c), and 10 (d). The dotted lines show the asymptotic expression (44).

It can be seen that the asymptotic expression is very close to the full solution for the whole parameter region calculated in the figure. For small α, $v_{\max}$ is close to the sound speed and v becomes close to $v_{\max}$ as soon as Δ becomes greater than Δ_G. On the other hand, for larger α, the crack speed v stays small until Δ gets close to σ_y.

(*5*) *Cohesive region length.* The numerically estimated length of the cohesive region ℓ is plotted against the crack speed v for δ/σ_y=0.001 and $\alpha = 0.1$ (a), 1 (b), 3 (c), and 10 (d) in Fig. 7 with the asymptotic expression (45). The cohesive region length ℓ becomes longer as v becomes larger except for the plots of $\alpha = 10$; in the $\alpha = 10$ case, ℓ gets shorter when v is close to 1, which is due to the factor $\sqrt{1-v^2}$ in Eq. (38), the "Lorentz contraction." ℓ becomes infinite at $v = v_{\max}$ for each α.

(*6*) *Crack opening.* The crack opening $U(x)$ is shown in Fig. 8 for $\delta/\sigma_y = 0.001$, $\alpha = 1$, and $v = 0.5$. The dashed line represents $U_0(x)$ for the case of $\sigma_c = 0$ and the dot-dashed lines show the slope $1-\chi = 1/2+\tan^{-1}\tilde{\alpha}$ and $2-\chi$, which take values of 0.667 and 1.667, respectively, for the parameters above. It can be seen that the crack openings for the $\sigma_c \neq 0$ case and the $\sigma_c = 0$ case are almost identical outside the cohesive zone, namely, outside the region of x where $U < \delta/\sigma_c = 0.001$ in the present case. The asymptotic behavior (27) for the $\sigma_c = 0$ case can be seen for $U \lesssim 0.1$ and the asymptotic behavior within the cohesive region for the $\sigma_c \neq 0$ case,

$$U(x) \sim x^{2-\chi} \qquad (x \to 0)\ , \tag{47}$$

is also seen.

It should be noted that the slope of $U(x)$ diverges logarithmically at $x = \ell$ as

$$U'(x) \sim -\ln|x-\ell| \qquad (x \sim \ell)\ , \tag{48}$$

due to the discontinuity of $\sigma_c(U)$ in the present simple form of the cohesion stress (36). This divergence will be absent if we use a continuous cohesive stress.

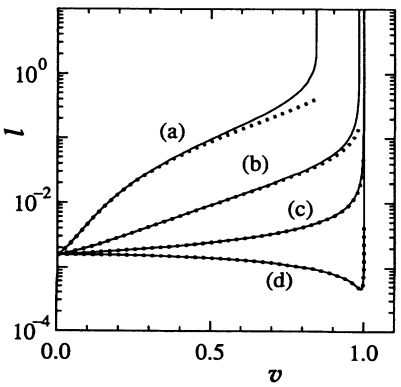

FIG. 7. The cohesive region length ℓ vs the crack speed v on a semilog scale for $\delta/\sigma_c = 0.001$ and α =0.1 (a), 1 (b), 3 (c), and 10 (d). The dotted lines show the asymptotic expression (45).

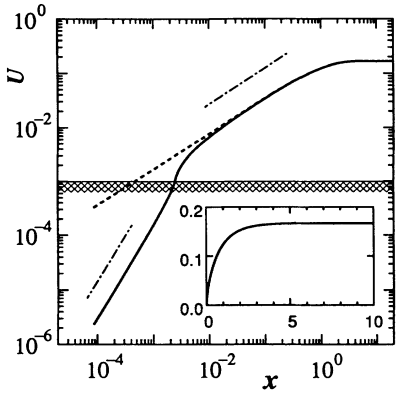

FIG. 8. The crack opening U vs x on a log-log scale and on a linear scale (inset) for $\alpha = 1$, $\delta/\sigma_c = 0.001$, and $v = 0.5$. The cohesive stress is operative below the shaded line, namely, for $U < \delta/\sigma_c$. The dashed line shows $U_0(x)$ for the case without cohesive stress. The dotted-dashed lines indicate the lines with slope $1-\chi$ (upper one) and $2-\chi$ (lower one).

VI. DISCUSSION

Both LN and we studied the effects of surface dissipation on crack propagation. The difference between their model and the present one is the origin of dissipation; in their model, the effect of surface dissipation comes from the surface viscosity; namely, the term $-\eta(\partial^2\dot{U}/\partial x^2)$ instead of the friction term $\alpha\dot{U}$ in Eq. (3). One of the physical situations where such friction may operate is an earthquake fault in a subduction zone, and the velocity strengthening friction should usually cause aseismic motion. For seismic motion, velocity weakening or slip weakening friction has to be considered, but the mathematical nature of the problem differs from the present one.

The velocity strengthening friction force acts as a traction force on the crack surface and the crack opening around the crack tip becomes $U_0(x) \sim x^{1-\chi}$ $(0 < \chi < 1)$, which is weaker than the ordinary $\sqrt{x}$ opening without traction. Since the stress singularity is a direct result of the crack opening, this weaker crack opening results in a weaker stress singularity $\sigma_0(x) \sim |x|^{-\chi}$ than the ordinary one. Note that there is no $1/\sqrt{x}$ region outside since the traction force due to the friction is operative over the whole crack surface.

The crack speed is determined by the condition that the stress at the crack tip should not diverge, or the so called "Barenblatt condition." If the crack speed does not satisfy this condition, the stress ahead of the crack tip diverges as $\sigma(x) \sim x^{-\chi}$ with $0 < \chi < 1/2$. This should be contrasted to the case with the viscosity term studied by LN, where a δ-function singularity at $x = 0$ appears if the crack speed does not satisfy the condition.

Let us discuss the parameter region that should be appropriate for most real situations. In the following, we use the original unit system. The parameter $W \equiv c_0/\omega_0$ is the length scale over which the externally applied distortion extends. The parameter δ is the maximum displacement where the cohesive stress is operative, and

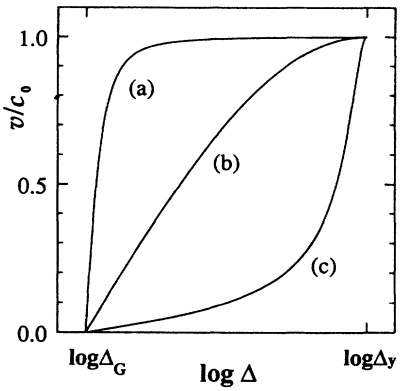

FIG. 9. The logarithm of the external load Δ vs the crack speed v in the $\mu\delta/W\sigma_y \to 0$ limit for $(W\omega_0/\mu)\alpha$ =0.1 (a), 1 (b), and 10 (c). The original unit system is used.

therefore the ratio $\mu\delta/W\sigma_y$ (or δ/σ_y in the dimensionless units) is the ratio of the stress that should appear if the external displacement were δ to the yield stress, in other words, the ratio of the cohesive region size to the displacement that would be needed to generate the yield stress σ_y without stress concentration. This ratio should depend on the physical situation but we expect it to be very small in general.

In this small $\mu\delta/W\sigma_y$ limit, the maximum crack speed $v_{\max}$ approaches the sound speed c_0 as may be seen from Eq. (43). It is important, however, to realize that this does not mean the effects of friction are negligible in this limit.

Consider the Δ dependence of the crack speed v. The speed v grows from 0 to $v_{\max}$ as Δ changes from Δ_G to $\Delta_y \equiv W\sigma_y/\mu$; thus, in the $\mu\delta/W\sigma_y \to 0$ limit, we obtain from Eq. (44)

$$\frac{\ln\Delta - \ln\Delta_G}{\ln\Delta_y - \ln\Delta_G} = \frac{2}{\pi}\tan^{-1}\left(\frac{W\omega_0}{\mu}\alpha\frac{v/c_0}{\sqrt{1-(v/c_0)^2}}\right), \tag{49}$$

where we present the expression in the form that the left hand side changes from 0 to 1 as v changes from 0 to c_0. This is plotted in Fig. 9 for $(W\omega_0/\mu)\alpha$ =0.1, 1, and 10.

As can be seen from the figure, for $\alpha \gtrsim \mu/W\omega_0$ the crack speed does not grow rapidly toward the sound speed c_0 after Δ exceeds Δ_G. The parameter value $\alpha \sim \mu/W\omega_0$ corresponds to the situation that the friction stress and the distortion stress are of the same order. Note that $d(v/c_0)/d(\Delta/\Delta_G) \to 0$ for any value of α in the limit of $\mu\delta/W\sigma_y \to 0$ because the ratio Δ_y/Δ_G diverges.

In conclusion, the surface dissipation can have important nontrivial effects on crack propagation.

ACKNOWLEDGMENT

The author thanks Professor J. S. Langer for his critical reading of the manuscript.

APPENDIX

The detailed derivation of the factorization (17)–(21) is given in this Appendix. $\hat{Q}(k)$ can be expressed formally as

$$\hat{Q}(k) = \exp[\ln\hat{Q}(k)] = \exp\left[\int_0^k dz\frac{\hat{Q}'(z)}{\hat{Q}(z)}\right]. \tag{A1}$$

Note that the last integral can be done in the complex z plane and depends upon the integral path from the origin to $z = k$. The path determines the branch to evaluate $\hat{Q}(k)$ on its Riemann surface.

Using the Cauchy formula, the integrand can be decomposed as

$$\frac{\hat{Q}'(z)}{\hat{Q}(z)} = \hat{f}^{(+)}(z) + \hat{f}^{(-)}(z) \tag{A2}$$

with

$$\hat{f}^{(\pm)}(z) \equiv \mp\int_{C^{(\pm)}}\frac{d\zeta}{2\pi i}\frac{1}{\zeta - z}\frac{\hat{Q}'(\zeta)}{\hat{Q}(\zeta)}, \tag{A3}$$

where $C^{(\pm)}$ in the complex ζ plane are the same as those indicated in Fig. 3.

Then we can proceed as

$$\begin{aligned}\hat{A}^{(\pm)}(k) &\equiv \int_0^k dz\hat{f}^{(\pm)}(z)\\ &= \mp\int_0^k dz\int_{C^{(\pm)}}\frac{d\zeta}{2\pi i}\frac{1}{\zeta - z}\frac{\hat{Q}'(\zeta)}{\hat{Q}(\zeta)}\\ &= \mp\int_{C^{(\pm)}}\frac{d\zeta}{2\pi i}\ln\left(\frac{\zeta}{\zeta - k}\right)\frac{\hat{Q}'(\zeta)}{\hat{Q}(\zeta)}.\end{aligned} \tag{A4}$$

Since the only singularities of $\hat{Q}'(\zeta)/\hat{Q}(\zeta)$ are a simple pole at $\zeta = k_0$ and cuts along the imaginary axis, the path $C^{(\pm)}$ can be deformed into the thick paths shown in Fig. 10. Using the fact that the integral along the circle with infinite radius vanishes, we obtain

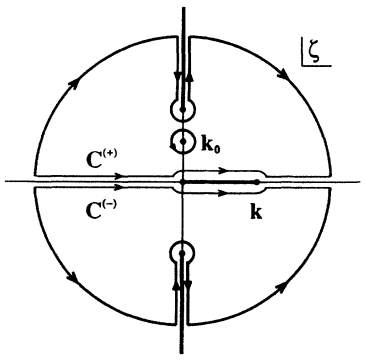

FIG. 10. The integral paths in the complex ζ plane to estimate Eq. (A4). The original paths $C^{(\pm)}$ can be deformed into the thick lines with arrows. The solid circle and the thick lines along the axes denote the pole and the cuts of the integrand of Eq. (A4).

$$\hat{A}^{(+)}(k) = -\ln\left(\frac{k_0}{k_0-k}\right) - \int_1^\infty \frac{dp}{2\pi}\ln\left(\frac{ip}{ip-k}\right) \times\left(\frac{\hat{Q}'(ip+\epsilon)}{\hat{Q}(ip+\epsilon)} - \frac{\hat{Q}'(ip-\epsilon)}{\hat{Q}(ip-\epsilon)}\right), \tag{A5}$$

$$\hat{A}^{(-)}(k) = -\int_1^\infty \frac{dp}{2\pi}\ln\left(\frac{ip}{ip+k}\right) \times\left(\frac{\hat{Q}'(-ip+\epsilon)}{\hat{Q}(-ip+\epsilon)} - \frac{\hat{Q}'(-ip-\epsilon)}{\hat{Q}(-ip-\epsilon)}\right), \tag{A6}$$

where ϵ is a positive infinitesimal. By performing partial integrations, these become

$$\hat{A}^{(+)}(k) = -\ln\left(\frac{k_0}{k_0-k}\right) - \int_1^\infty \frac{dp}{\pi}\left(\frac{1}{p} - \frac{1}{p+ik}\right)\theta(p), \tag{A7}$$

$$\hat{A}^{(-)}(k) = \int_1^\infty \frac{dp}{\pi}\left(\frac{1}{p} - \frac{1}{p-ik}\right)\theta(p), \tag{A8}$$

with

$$\theta(p) \equiv \tan^{-1}\left(\frac{\sqrt{p^2-1}}{\tilde{\alpha}p}\right), \tag{A9}$$

and this completes the factorization.

[1] L.B. Freund, *Dynamic Fracture Mechanics* (Cambridge University Press, New York, 1990).

[2] K. Ravi-Chandar and W.G. Knauss, Int. J. Fract. **26**, 141 (1984).

[3] J. Fineberg, S.P. Gross, M. Marder, and H.L. Swinney, Phys. Rev. Lett. **67**, 457 (1991).

[4] K. Sieradzki, G.J. Dienes, A. Paskin, and B. Massoumzadeh, Acta Metall. **36**, 651 (1988).

[5] M. Barbar, J. Donley, and J.S. Langer, Phys. Rev. A **40**, 366 (1989).

[6] J.S. Langer and C. Tang, Phys. Rev. Lett. **67**, 1043 (1991).

[7] J.S. Langer, Phys. Rev. A **46**, 3132 (1992).

[8] C. Myers and J.S. Langer, Phys. Rev. E **47**, 3048 (1993).

[9] J.S. Langer and H. Nakanishi, Phys. Rev. E **48**, 439 (1993). This paper will be referred to as LN in the present paper.

[10] M. Marder and X. Liu, Phys. Rev. Lett. **71**, 2417 (1993).

[11] E.S.C. Ching (unpublished).

[12] For a general description of the Wiener-Hopf technique, see, for example, P.M. Morse and H. Feshbach, *Methods of Theoretical Physics* (McGraw-Hill, New York, 1953), Pts. 1 and 2.